Dampened regulates the activating potency of Bicoid and the embryonic patterning outcome in *Drosophila*

Junbo Liu[1] and **Jun Ma**[1,2,*]

[1] Division of Biomedical Informatics Cincinnati Children's Research Foundation 3333 Burnet Avenue Cincinnati, Ohio United States of America

[2] Division of Developmental Biology Cincinnati Children's Research Foundation 3333 Burnet Avenue Cincinnati, Ohio United States of America

Abstract

The *Drosophila* morphogen gradient of Bicoid (Bcd) initiates anterior-posterior (AP) patterning, but it is poorly understood how its ability to activate a target gene may impact this process. Here we report an F-box protein, Dampened (Dmpd) as a nuclear co-factor of Bcd that can enhance its activating potency. We establish a quantitative platform to specifically investigate two parameters of a Bcd target gene response, expression amplitude and boundary position. We show that embryos lacking Dmpd have a reduced amplitude of Bcd-activated *hunchback* (*hb*) expression at a critical time of development. This is due to a reduced Bcd-dependent transcribing probability. This defect is faithfully propagated further downstream of the AP patterning network to alter the spatial characteristics of *even-skipped* (*eve*) stripes. Thus, unlike another Bcd-interacting F-box protein Fates-shifted (Fsd), which controls AP patterning through regulating the Bcd gradient profile, Dmpd achieves its patterning role through regulating the activating potency of Bcd.

Introduction

Embryonic patterning along the anterior-posterior (AP) axis of the *Drosophila* embryo is initiated by the action of the morphogenetic protein Bicoid (Bcd) [1,2]. Bcd is a transcriptional activator that stimulates the expression of AP patterning genes [3,4]. One such gene is *hunchback* (*hb*), which, in response to the Bcd concentration gradient, has an expression domain in the anterior half of the embryo [5,6]. It is well documented that, based on morphological and molecular markers, altering the *bcd* gene dose maternally can shift the fatemap landscape in the embryo [7,8]. Experimental perturbations of the Bcd gradient properties such as the profile shape and precision can cause corresponding changes in the

*Corresponding author: Divisions of Biomedical Informatics and Developmental Biology, Cincinnati Children's Hospital Research Foundation, 3333 Burnet Avenue, Cincinnati, OH 45229, USA; 513-636-7977 (phone); jun.ma@cchmc.org.

expression boundary of *hb*, further supporting a threshold-dependent action of Bcd in transcriptional activation during development [3,4,7,9-11]. Aside from its concentration-dependent action, there is another property of Bcd that is inherent to a transcriptional activator, namely, its ability (or potency) to activate target gene transcription. There have been studies investigating the activation domains of Bcd and the regulation of its activity [12-17]. However, it remains unknown—owing in part to a lack of adequate quantitative tools in the earlier studies—how the activating potency of Bcd may specifically impact the AP patterning network at a mechanistic level.

F-box proteins play important regulatory roles in many molecular and cellular processes [18-22]. These proteins often exist as subunits of the SCF (Skp1–Cul1/Cdc53–F-box protein)-type ubiquitin E3 ligases, representing the specificity determinants of these protein complexes [22-24]. A well-documented function of F-box proteins is their ability to bind specifically to protein substrates and target them for ubiquitination and proteasome-mediated degradation. In a recent study, we reported the identification of a novel F-box protein, Fate-shifted (Fsd), that has a role in targeting Bcd for ubiquitination and degradation [10]. Embryos mutant for *fsd* have an altered (elongated) Bcd gradient profile and, as a result, a posterior shift in *hb* expression boundary and the entire fatemap. These results provide a fresh example illustrating the important roles of F-box proteins in regulating developmental fate specification.

In addition to the regulation of substrate stability, F-box proteins have also emerged to have an ability to stimulate the activity of transcription factors [25-27]. For example, the F-box protein Skp2 can act as a co-activator for c-Myc-induced transcription in addition to regulating c-Myc stability [28,29]. Another F-box protein, β-TrCp1/Fbw1a, has been shown to enhance the ability of β-catenin to activate transcription through cooperating with the co-activator p300 in addition to targeting β-catenin for degradation [30]. We were interested in understanding whether the activating potency of Bcd might be subject to regulation by F-box proteins. A major motivation of our interest in this question lied at the promise that the Bcd gradient system should be suitable for dissecting the mechanistic details of transcriptional regulation in a native biological system with fine resolutions both temporally and spatially. Our analysis of Fsd indicated that this F-box protein does not regulate the activating potency of Bcd (see below for details), which is consistent with the fact that Fsd is predominantly localized to the cytoplasm [10].

Here we present studies of another novel F-box protein, encoded by *dampened* (*dmpd*, CG11866), which is a nuclear co-factor of Bcd. We show that embryos from females mutant for *dmpd* have a decreased *hb* mRNA level at nuclear cycle (nc) 14, a defect that can be traced back to a reduction in *hb* transcribing probability (hence the gene name *dampened*). The lowered amplitude (level) of *hb* expression can be propagated into the AP patterning network to alter the spacing of *even-skipped* (*eve*) stripes that are sensitive to absolute concentrations of Hb. These results demonstrate that the activating potency of Bcd is subject to regulation for the embryo to achieve a normal AP patterning outcome. The contrasting properties of Fsd and Dmpd also illustrate that two distinct properties of Bcd as a morphogen—its concentration gradient profile and its ability to activate transcription—are subject to regulation by distinct F-box proteins.

Results

Nuclear F-box protein Dmpd regulates Bcd activity

In our efforts to study the roles of F-box proteins in regulating Bcd functions, we identified Dmpd as a nuclear co-factor of Bcd. Figs. 1a and 1b show the results of a co-immunoprecipitation (co-IP) assay, where we co-transfected the human embryonic kidney (HEK) 293T cells with plasmids expressing HA-tagged Bcd (HA-Bcd) and FLAG-tagged Dmpd (FLAG-Dmpd). HEK293T cells are widely used as a host system to study F-box protein functions [10,31]. Here we used anti-HA antibody to pull down HA-Bcd in co-IP and anti-FLAG antibody to detect FLAG-Dmpd in Western blots (see Figs. 1a and 1b, lanes 5 and 6, for control experiments documenting antibody specificity). Fig 1a shows the Western blot results where FLAG-Dmpd was specifically co-precipitated by HA–Bcd (lane 4; see other lanes for controls). In a reciprocal setting, where anti-FLAG antibody was used to pull down FLAG-Dmpd in co-IP and anti-HA antibody was used to detect HA-Bcd in Western blots, we obtained equivalent results (Fig. 1b, lane 4, see other lanes for controls), further documenting an interaction between HA-Bcd and FLAG-Dmpd.

Immunocytochemistry in *Drosophila* S2 cells reveals that Dmpd is almost exclusively localized to the nucleus (Figs. 1d-f), suggesting that it may play a role in regulating the function of Bcd as a transcription activator. To test this possibility, we used a reporter gene encoding chloramphenicol acetyltransferase (*CAT*) under the control of the ~250bp Bcd-responsive native *hb* enhancer element [13,32,33]. Fig. 1c shows that the CAT reporter activity was increased ~1.7 fold by the expression of Dmpd in cells. To determine whether the action of Dmpd on reporter activation might be through a general mechanism that is independent of Bcd, we performed reporter assays where the reporter expression is activated by an artificial transcription activator Gal4-VP16 [34]. Our results (Fig. 1c) show that the reporter activity in this case was not increased by Dmpd expression in cells, excluding the possibility that Dmpd stimulates transcription through a general mechanism that is independent of Bcd.

Evaluating *hb* expression boundary and amplitude

To evaluate the impact of Dmpd on Bcd-activated transcription in a native developmental context, we first sought to establish a quantitative platform suitable for simultaneously but specifically evaluating the two parameters of a response to the Bcd input: the amplitude and boundary position of *hb* expression in the embryo. While previous studies in *Drosophila* embryos have focused extensively on the regulation of *hb* expression boundary [11,35-40], relatively little attention has been paid to the regulation of the amplitude of Bcd target gene expression. We chose *hb* for evaluating the regulation of Bcd activating potency because, unlike most AP patterning genes which also respond to other inputs [41,42], *hb* responds primarily to the Bcd input [9,43], which should make it a sensitive target suitable for such evaluations. Gap genes such as *hb* are located at the top of the hierarchy of the regulatory cascade of the AP patterning network to establish the earliest interpretations of the maternal inputs. For our experiments, we used quantitative fluorescence *in situ* hybridization (FISH) to detect mature *hb* mRNA in the cytoplasm of the blastoderm embryo. To maintain a linear relationship between the fluorescence signal intensity and *hb* mRNA level, we avoided any non-linear signal amplification steps and ensured that all images were captured within a

linear range. In addition, for any comparisons to be made, all the experimental and imaging steps were performed on a side-by-side basis. Under these conditions, the un-normalized, raw fluorescent intensities should allow us to compare directly the *hb* mRNA levels among different groups of embryos and, as detailed below, we used calibrating embryos to specifically validate this point. To process the captured images, we first extracted the FISH intensities at locations within the basal cytoplasmic layer along the dorsal side of an embryo. The extracted intensity data were then projected to the AP axis and expressed as a function of fractional embryo length *x/L*. For our study, we defined the *hb* expression boundary, x_{hb}, as the AP position at which the detected FISH intensity is at half maximal. We quantify the amplitude of Bcd-activated *hb* expression through the use of hb_{plat}, which denotes the averaged un-normalized, raw intensity at positions in the plateau region of the anterior *hb* expression domain of an embryo [44].

We used calibrating embryos to test and validate our quantitative platform outlined above. These embryos have one, two or four copies of the *hb* gene (referred to as 1×, 2× and 4×*hb* embryos, respectively). Here side-by-side quantitative FISH experiments were performed in these embryos to detect and quantify mature *hb* mRNA. To ensure reliable comparison of *hb* expression properties, embryos were specifically selected to be at a time (~5-15 min into nc 14) when hb_{plat} is known to have reached its stable, peak levels [44]. The only adjustment in our analysis was an embryo-specific background subtraction step that eliminated embryo-to-embryo differences in terms of background fluorescence. Fig. 2a shows the mean *hb* intensity profiles from 1×, 2× and 4×*hb* calibrating embryos (see Supplementary Fig. S1 for individual intensity profiles). These profiles exhibit a classical and well-documented sigmoidal shape, each with a sharp boundary. Fig. 2b shows that the mean hb_{plat} values exhibit a linear relationship with the *hb* copy number ($hb_{plat} = 5.00*c + 0.86$, where *c* is *hb* copy number; *R* squared for linear regression $R^2 = 0.75$). These results show that hb_{plat} detected under our experimental and analytical framework is a sensitive and reliable measure of the mature *hb* mRNA level and thus a valid parameter for quantifying the amplitude of a Bcd target gene response in the embryo.

Since *hb* expression is dependent on Bcd function, we sought to further document in an unambiguous manner whether hb_{plat} is, or is not, sensitive to changes in *bcd* gene copies. Here, our goal was to document specifically whether hb_{plat} is sensitive to the *hb* boundary position or not. We performed quantitative FISH to detect *hb* mRNA in embryos from females that have one, two or three copies of the *bcd* gene (referred to as 1×, 2× and 3×*bcd* embryos, respectively; see Supplementary Fig. S2 for individual intensity profiles). Figs. 2c and 2d show our quantitative data. They confirm that x_{hb} is a function of *bcd* gene copy number, exhibiting a progressive posterior shift as the *bcd* gene copy number increases. However, the mean hb_{plat} values remain similar in 1×, 2× and 3×*bcd* embryos (Fig. 2d). These results further document that hb_{plat} quantifies exclusively how much *hb* mRNA is produced irrespective of where its expression boundary is located in the embryo. They provide further confirmation that hb_{plat} is a valid and specific parameter for quantifying the amplitude of a Bcd target gene response.

dmpd mutation reduces *hb* mRNA level in the embryo

With the established quantitative platform outlined above, we proceeded to investigate the potential role of Dmpd in regulating the activating potency of Bcd during development. For this purpose, we generated a deletion allele *dmpd^6-3* through P-element mediated imprecise excision using a publicly available insertion line (Bloomington fly stock 17518). The resulting *dmpd^6-3* allele has a 3106 bp deletion covering almost the entire coding region of *dmpd* (Fig. 3a). It is homozygous viable at 25°C, which made it possible for us to directly collect embryos from homozygous *dmpd^6-3* females. Using our quantitative tools described above, we evaluated specifically the effect of the *dmpd* mutation on *hb* mRNA profiles in the embryo. Here we performed quantitative FISH in embryos from *w^1118* or *dmpd^6-3* mothers, referred to as wt and *dmpd* embryos, respectively. Fig. 3b shows the mean profiles of *hb* mRNA FISH intensities (raw, background-subtracted) from wt and *dmpd* embryos (see Supplementary Fig. S3 for individual profiles), revealing a lower intensity level in *dmpd* embryos. Fig. 3c shows that $hb_{plat} = 30.98 \pm 6.18$ [all values given in this report are mean ± standard deviation (sd) unless stated otherwise; $n = 22$] and 18.10 ± 5.10 ($n = 18$) in wt and *dmpd* embryos, respectively ($p = 2.04 \times 10^{-8}$; all p values given in this report are from Student's t-tests unless stated otherwise), documenting a significant reduction in Bcd-activated *hb* expression amplitude in *dmpd* embryos. The observed defect of *dmpd* embryos in *hb* amplitude reduction is Bcd-dependent because the amplitude of the posterior *hb* expression domain, which is driven by a Bcd-independent enhancer [45], was unaffected ($hb_{post} = 9.99 \pm 5.77$ and 10.14 ± 4.36 in wt and *dmpd* embryos, respectively; $p = 0.93$; see Fig. 3C for hb_{post} definition). In addition, the embryos chosen in our evaluation of *hb* mRNA levels are at early nc 14 since the *hb* expression stripe at parasegment 4 (PS4), which is dependent on gap gene cross-regulatory inputs [36,45], has not yet gained any appreciable prominence (Fig. 3b). Together, these findings suggest that the activating potency of Bcd is subject to positive regulation by Dmpd during development.

To evaluate the specificity of our *dmpd* deletion allele, we performed the following two sets of experiments. First, we compared hb_{plat} between wt embryos and those from *dmpd^6-3/ Df(2R)BSC303* females (referred to as *dmpd/Df* embryos). *Df(2R)BSC303* is a small deficiency (~70kb) that removes the entire *dmpd* coding region. Our results (Supplementary Fig. S4) show that, similar to *dmpd* embryos, *dmpd/Df* embryos also have a reduced hb_{plat}, from 25.05 ± 5.47 ($n = 10$) in wt embryos to 17.93 ± 4.03 ($n = 12$) in *dmpd/Df* embryos ($p = 2.20 \times 10^{-3}$). Second, we backcrossed *dmpd^6-3* females with *w^1118* males for six generations to establish a *dmpd^6-3* line in *w^1118* background, referred to as *dmpd^6-3w*. We performed quantitative *hb* FISH in embryos from *w^1118* or *dmpd^6-3w* females, further confirming a reduction in hb_{plat} in *dmpd^6-3w* embryos (Supplementary Fig. S5). In both sets of experiments, hb_{post} was unaffected (Supplementary Figs. S4f and S5f). Together, these results document that the observed hb_{plat} reduction is a defect that is caused specifically by the *dmpd* mutation (as opposed to genetic background differences). They further support a role of Dmpd in stimulating specifically Bcd-dependent *hb* transcription in the embryo.

dmpd mutation alters AP patterning characteristics

Hb regulates AP patterning by controlling the expression boundaries of downstream genes in a concentration-dependent manner [16,17,46]. Specifically, the spacing between the anterior

boundaries of *even-skipped* (*eve*) stripes 3 and 4 (referred to as $EL_{\text{eve3-4}}$) is known to be controlled by the absolute Hb concentrations in the embryo [47,48]. A reduction in the absolute Hb level (in *hb*/+ heterozygous embryos) has a well-documented consequence of enlarging $EL_{\text{eve3-4}}$ [47,48]. To determine whether the effect of Dmpd on *hb* transcription (i.e., the reduced amplitude) can be propagated further downstream of the AP patterning network, we performed quantitative FISH to detect *eve* expression patterns in wt and *dmpd* embryos for a direct comparison of $EL_{\text{eve3-4}}$. Fig. 4a shows the mean intensity profiles of *eve* in wt and *dmpd* embryos (see Supplementary Fig. S6 for individual profiles). Fig. 4b shows the measured $EL_{\text{eve3-4}}$ in these embryos, documenting a significantly larger $EL_{\text{eve3-4}}$ in *dmpd* embryos [(7.60 ± 0.37% embryo length (EL), $n = 13$] than in wt embryos (6.34 ± 0.45% EL, $n = 16$; $p = 9.26 \times 10^{-9}$). These results show that the impact of the reduced amplitude of *hb* expression caused by the *dmpd* mutation can be faithfully propagated downstream of the AP patterning network, indicating a role of Dmpd in specifying a normal AP patterning outcome.

dmpd reduces *hb* transcribing probability at nc 14

Our study described thus far shows that Dmpd can enhance the activating potency of Bcd and is required for a normal AP patterning outcome. To investigate at a deeper mechanistic level how Bcd-activated *hb* transcription becomes compromised in *dmpd* embryos, we employed a technique that we developed recently for monitoring active *hb* transcription [44]. Here, we used an intronic probe to detect the nascent *hb* transcripts near the Bcd-responsive P2 promoter (see Figs. 5a and 5b for images of a wt embryo at nc 14). Since the 283bp *hb* intron is very close to the P2 promoter (145bp downstream) and since RNA intron sequences are believed to be quickly removed upon being transcribed [49], our technique permits a close monitoring of the transcriptional status of individual *hb* gene copies near the Bcd-responsive promoter. In our analysis, the fluorescence dots detected inside the nucleus (referred to as the intron dots) represent individual copies of *hb* undergoing active transcription in snapshots of the embryos. For each embryo, we first calculated the mean intron dot number per nucleus (ρ) at positions along the AP axis (Fig. 5c). This parameter quantifies the probability of *hb* gene copies undergoing active transcription (referred to as transcribing probability) at an AP position in a snapshot of the embryo. Specifically, ρ = 2 indicates that all *hb* copies in the nuclei at the AP position under investigation are actively transcribing in the snapshot, thus denoting a transcribing probability of 100%. To specifically evaluate Bcd-activated *hb* transcription, we also calculated the average ρ for positions in the plateau region of the *hb* expression domain, ρ_{plat} [44]. To minimize the effects of both PS4 and the variable anterior stripe [6,45] on the calculation of ρ_{plat}, the plateau region was chosen to be a domain that spans 10% EL and has a posterior boundary that is ~10% EL anterior to the detected *hb* expression boundary of the embryo. The parameter ρ_{plat} thus provides a quantification of the maximal Bcd-dependent transcribing probability of *hb* gene copies in a snapshot of the embryo.

To obtain an accurate comparison of *hb* transcribing probability between wt and *dmpd* embryos, we grouped embryos into well-resolved temporal classes. These time classes have a temporal resolution of ~1 min with an uncertainty of ~0.6-~0.9 min [44]. Figs. 5d-i show the mean ρ profiles in wt and *dmpd* embryos at time classes from t1 to t6 (see Supplementary

Figs. S7 and S8 for individual profiles). These profiles show a reduced ρ level at time classes t3-t6, which represent embryos that are ~3 to ~6 min into nc 14 interphase (see Discussion for ρ properties at t1 and t2). For example, the peak transcribing probability is reached in wt embryos at t3 with a mean ρ_{plat} of 1.03 ± 0.08 ($n = 7$). By contrast, *dmpd* embryos at this time class have a significantly lower transcribing probability with a mean ρ_{plat} of 0.79 ± 0.21 ($n = 5$; $p = 1.6 \times 10^{-2}$; see Fig. 5 legend for p values for other time classes). These results uncover an underpinning defect caused by the *dmpd* mutation, namely, a reduction in the transcribing probability of individual copies of the *hb* gene in the embryo. Importantly, the estimated contributions of active *hb* transcription at PS4 are insensitive to *dmpd* mutation in embryos that have developed a detectable PS4 stripe in the form of intron dots (see Supplementary Fig. S9 and legend). It is worth mentioning that, while the roles of co-factors in modulating the transcriptional outcome are well documented [50], our finding that Dmpd regulates the transcribing probability of a native Bcd target gene in a native developmental system represents a significant advancement in our understanding of mechanisms of transcriptional regulation.

dmpd does not affect Bcd gradient profile

F-box proteins can enhance activator function through a variety of mechanisms [27,51-53]. They can be either proteolytic or non-proteolytic in nature as defined by their ability to regulate activator stability. To investigate whether Dmpd has a role in regulating Bcd degradation in addition to its co-activator function, we evaluated the Bcd gradient properties in *dmpd* embryos. Here we performed quantitative immunostaining to detect Bcd protein in wt and *dmpd* embryos [10,11]. We extracted raw Bcd intensity without any adjustments, *B*, at different positions along the AP axis for individual embryos (see Supplementary Fig. S10 for the mean and individual profiles of Bcd intensities). According to a simple diffusion model, the length constant of an exponential Bcd gradient profile, λ, is a function of the diffusion constant *D* and degradation rate ω: $\lambda^2 = D/\omega$ [38,54]. In *dmpd* embryos, *D* is expected to be unchanged since Bcd itself is not altered, thus making it possible to use the estimated parameter λ to evaluate a potential impact of *dmpd* mutation on ω. Fig. 6a shows $ln(B/B_{max})$ plots for the mean Bcd intensity profiles from wt and *dmpd* embryos (normalized to their respective mean maximal *B* value, B_{max}) as a function of *x/L* (see Fig. 6 legend for further details). Here the logarithmic conversion transforms an exponential profile to a linear profile, where λ is the negative reciprocal of the slope. Our results show that the two linear fits have a similar slope, suggesting a similar λ between wt and *dmpd* embryos. In a second analysis, we calculated λ values of Bcd gradient profiles from individual embryos (see Methods for details). Our results further confirmed the similarity of the length constant, $\lambda = 72.96 \pm 11.52$ μm ($n = 15$) and 74.14 ± 12.56 μm ($n = 13$) in wt and *dmpd* embryos, respectively ($p = 0.80$; Fig. 6b). Together, these results suggest that, under the framework of a simple diffusion model, Dmpd does not have a significant role in regulating Bcd stability in embryos. They are supportive of a non-proteolytic role of Dmpd in enhancing the activating potency of Bcd.

Discussion

Morphogen gradients such as that of Bcd are excellent experimental paradigms for dissecting the mechanistic operations of the regulatory networks that control patterning decisions. They provide a unique window to probing the regulatory impacts of F-box proteins both spatially and temporally at a fine resolution. Increasing evidence supports the notion that F-box proteins—there are up to 45 of them in *Drosophila* and 75 in humans [55]—belong to a critical class of regulatory proteins, but few of them have been studied in native developmental contexts. In this work, we report the identification of a nuclear co-factor of Bcd, Dmpd that can enhance the potency of Bcd as an activator. Dmpd thus joins an expanding list of F-box proteins that can act as transcriptional co-activators [28-30]; it remains to be determined whether the co-activator role of Dmpd for Bcd in the embryo is dependent on a functional SCF complex and the E3 ligase activity. Our results show that embryos lacking Dmpd have a lower amplitude of Bcd-activated *hb* expression, a defect that can be passed further downstream of the network, causing an enlargement of $EL_{eve3\text{-}4}$, the spacing between *eve* expression stripes that are sensitive to absolute concentrations of Hb. In embryos that lack another Bcd-interacting F-box protein Fsd, neither the *hb* expression amplitude nor $EL_{eve3\text{-}4}$ is affected (Supplementary Fig S11). This stems from the fact that, unlike Dmpd, Fsd regulates the Bcd gradient profile through a proteolytic pathway without a detectable co-activator function (ref [10] and Supplementary Fig S11). The contrasting functions of these two F-box proteins thus document that a normal AP patterning outcome is subject to regulation by two distinct mechanisms. These mechanisms control two distinct properties of Bcd that are indispensable to its morphogen action: the formation of a concentration gradient and the activation of its target genes.

A critical feature of morphogen gradients is their ability to induce downstream responses in a concentration-dependent manner. This particular feature has been subject to extensive investigations, in part because of a significant interest in the question of what morphogen gradients do. It has been proposed recently that the concentration-dependent input-output relationship between Bcd and *hb* also contributes directly to the formation of AP patterns that are scaled with the length of the embryo [11,56-58]. By contrast, the regulation of the amplitude of a response to the morphogen input has been relatively under-explored. Its importance may be better appreciated from the perspective of regulatory networks that control the patterning outcome. In the case of *hb* as a direct target gene of Bcd, its encoded protein Hb acts as an input, in a concentration-dependent manner [47,48], for genes (such as *eve*) that are further downstream of the AP patterning network. The regulation of the expression of these downstream genes allows the regulatory network to refine and evolve toward the desired final outcome of patterning. Since these downstream genes respond to absolute concentrations of Hb, the boundary position for *hb* expression in response to the Bcd gradient input has become no longer directly relevant to the decision-making processes of these genes. But as shown by our study, another feature of the *hb* response to the Bcd gradient input, namely its expression amplitude, remains directly relevant to the continued operation of the AP patterning network.

Our analysis of the impact of the *dmpd* mutation on active *hb* transcription reveals important mechanistic insights into the regulation of the transcription process in a native

developmental context. As documented recently [44], Bcd-activated *hb* transcription becomes detectable immediately upon entering the nc 14 interphase, but it is shut off within a few minutes. Our intron staining results (Figs. 5d and 5e) show that, at time classes t1 and t2, the *hb* transcribing probability at the plateau region is largely unaffected by the *dmpd* mutation (see Fig. 5 legend for ρ_{plat} and p values). They suggest that the onset of active *hb* transcription upon entering the nc 14 interphase is largely insensitive to *dmpd* mutation. The reduction in ρ_{plat} at t3 and subsequent time classes is thus consistent with the possibility that *dmpd* embryos might have a hastened shutdown of active *hb* transcription at the nc 14 interphase. To test this possibility, we performed quantitative *hb* mRNA FISH in wt and *dmpd* embryos with an exclusive focus on nc 13. Embryos at this stage already have a significant accumulation of *hb* mRNA suitable for quantitative measurements that are necessary for effective comparisons between wt and *dmpd* embryos. In addition and importantly, active *hb* transcription is known to span the entire interphases prior to nc 14 [44,59]. Thus, if the defect of *dmpd* embryos is specific to *hb* shutdown at the nc 14 interphase, *hb* mRNA level should remain unchanged prior to this shutdown, i.e., at nc 13. This prediction is supported by our results shown in Supplementary Fig. S12. An implication of these findings is that altering the *hb* expression amplitude at, and only at, the last interphase (nc 14) prior to cellularization and gastrulation can still impact the AP patterning outcome, suggesting that this interphase represents a critical time period in making patterning decisions forward.

An important feature of developmental systems is that their desired spatial properties must be attained within the allotted periods of time when an entire system is progressing along the irreversible temporal axis. This interconnection between the spatial and temporal aspects of the developmental systems poses significant constraints on their operation. In *Drosophila*, the early embryo undergoes rapid cycles of nuclear division [60]. This poses a constraint on the transcription process itself and the decoding of maternal gradient inputs since mitosis is known to abort transcription [61,62]. It has been documented that active *hb* transcription can resume almost immediately upon entering the interphase in the blastoderm embryo [44,59], but it remains unknown precisely how this can be achieved [61]. For developmental systems evolving rapidly along the temporal axis such as the early *Drosophila* embryo, patterning decisions may need to be made before true steady states could be achieved. In a recent study [63], it was shown that how quickly a gene can resume efficient transcription upon entering the nc 14 interphase can affect the amount (the amplitude) of the gene products at a later time when such products are needed for action. Thus, it was shown that a slowed onset of *snail* transcription led to gastrulation defects [63]. In the case of *dmpd* mutation investigated in this report, while the onset of active *hb* transcription upon entering the nc 14 interphase is unaffected, a hastened shutdown reduces the amplitude of *hb* expression products, a defect that alters the spatial characteristics of the patterning outcome (Fig. 4). Together, these two latest examples of dynamic regulation of transcription illustrate the importance of understanding the actual transcriptional decisions in a developmental system through the prism of time, an area of research that has only begun to be explored.

Three recent studies have reported investigations of the dynamics of transcription in early embryos. Two of the studies [64,65] were based on a live-imaging technique using the MS2

coat protein (MCP) system [66,67]. For evaluating the onset of transcription upon entering an interphase, the use of this system requires an adjustment by the delay between transcription initiation and detection of fluorescent signals at the reporter locus, as dictated by the time necessary for RNA polymerase to transcribe through the MS2 stem loop repeats and for the MCP-GFP protein to bind to these RNA repeats. With this and detection limit-imposed delay adjustments, both of the live-imaging studies are consistent with a quick onset of Bcd-dependent transcription initiation upon entering an interphase as documented in our current study and previous studies [44,59]. The live-imaging study of Lucas et al. [64], also supports a role of Bcd in directly lengthening the time period of active transcription during an interphase. At the nc 14 interphase, both the live-imaging study of Garcia et al. [65] and a third study of Little et al. [68] that was performed on fixed embryos support a shutdown of *hb* transcription that we initially reported [44] and further investigated in the current study. The results of Garcia et al. [65], when adjusted by the method-dictated time delays, are also broadly consistent with our estimated kinetics of *hb* shutdown. Importantly, the observation [65] that a reporter gene driven by the ~250bp Bcd-responsive *hb* enhancer element [13,32,42] is shut down at nc 14 in a manner that is broadly similar to the endogenous *hb* shutdown is consistent with our documented role of Dmpd and the activating potency of Bcd in influencing this shutdown process. Finally, we note that the dynamic properties of *hb* shutdown described by Little et al. [68] contradict with both our findings [44] and those of Garcia et al. [65]. Unlike our experimental and analytical framework designed to evaluate specifically the dynamics of transcription initiation or elongation near the Bcd-dependent promoter [43,44,69], the active *hb* loci detected by Little et al. [68] monitor the "aggregate" transcription status along the entire *hb* gene length detected by the probes. This makes the fluorescent signal intensities at the active *hb* loci as an insensitive quantity in studying the dynamics of *hb* shutdown at nc 14. In particular, the use of this quantity as transcription activity likely has contributed to the reported mismatch between ~30% reduction in "transcription activity" and ~3 fold reduction in cytoplasmic *hb* mRNA counts from early to late embryos at nc 14. These results support a suggestion that, upon the sharp (in magnitude) and quick (in time) shutdown of *hb* transcription at early nc 14 as documented by our method [44], the lingering signals at the "active" *hb* loci [68] are largely unrelated to transcription initiation or elongation near the Bcd-dependent promoter.

A contribution of our current work is the establishment of a quantitative platform for specifically (and simultaneously) analyzing the amplitude and expression boundary of a target response to the Bcd gradient input. Under our current experimental framework, these two parameters are primarily subject to regulation by two distinct mechanisms. Our results document that Dmpd has a role in enhancing the activating potency of Bcd as an activator and in regulating the AP patterning outcome. Interestingly, we observe a detectable, though small, posterior shift in x_{hb} in *dmpd* embryos (see Fig. 3, Supplementary Figs. S4 and S5, and their legends), suggesting that Dmpd may have regulatory roles beyond its primary role of regulating the amplitude of *hb* expression. This posterior shift in x_{hb} cannot be simply explained by the Bcd gradient profile properties because a smaller B_0 (Bcd concentration at the anterior) in *dmpd* embryos, if biologically meaningful, would have predicted a small shift in x_{hb} toward the anterior. This small shift is detectable in embryos not yet exhibiting a significant sign of PS4 expression (Fig. 3), suggesting that it is related to Bcd-dependent *hb*

transcription. It remains to be determined mechanistically whether Dmpd may have a meaningful role in regulating the affinity of Bcd for the *hb* enhancer during development. We anticipate that, as we develop more experimental tools and identify more regulatory players, we will be able to further improve our mechanistic knowledge about how the AP patterning network operates in space and time at an even finer resolution and precision.

Methods

Plasmids and lines of cells and flies

Plasmids were constructed with standard DNA cloning methods. To express proteins in *Drosophila* S2 cells and human embryonic kidney (HEK) 293T cells, the corresponding cDNA sequences were cloned into the pAc5.1/V5-His C and pcDNA3 vectors, respectively. The following plasmids were from our previous studies [10,13]: FY441 expressing HA-Bcd from the pGEM3 vector, FY442 expressing HA-Bcd from the pAc5.1/V5-His C vector, and ljb3087 expressing HA-Bcd from the pcDNA3 vector. The sequence encoding FLAG-tagged Dmpd was PCR amplified from a *dmpd* cDNA-containing clone (GM04147; the *Drosophila* Genomics Resource Center) with the following primers: 5'-GAC TAC AAG GAC GAC GAT GAC AAG ATG GTG TCC ACC CGC CAA ATG-3' (FLAG-tagged Dmpd primer) and 5'-TGC TCT AGA TTA TTT ACT GCG TTT GCC GGG-3'. The PCR product was digested with Xba I and ligated with the pGEM3 vector derived from FY441 that had been digested with Nco I, treated with Klenow fragment of DNA polymerase I, and digested subsequently with Xba I. The resulting intermediate plasmid, ljb4048, was then digested with Hind III and Xba I to yield a fragment (encoding FLAG-Dmpd) that was ligated with the pAC5.1/V5-His C and pcDNA3 vectors derived from Hind III and Xba I digestions of FY442 and ljb3087, respectively. The resulting plasmids ljb4049 and ljb4102 were used to express FLAG-Dmpd in *Drosophila* S2 and HEK293T cells, respectively. To obtain the plasmid (ljb4096) expressing HA-Dmpd in *Drosophila* S2 cells, the same cloning strategy for ljb4049 was used except the use of an HA-tagged Dmpd primer (5'-GCT TAC CCA TAC GAT GTT CCA GAT TAC GCT ATG GTG TCC ACC CGC CAA ATG-3') in place of the FLAG-tagged Dmpd primer.

Drosophila S2 cells and HEK293T cells were grown in Schneider's *Drosophila* medium (Invitrogen) at room temperature and Dulbecco's modification of Eagle's medium (Cellgro) at 37°C, respectively. Both media contained 10% (v/v) fetal calf serum (Invitrogen) and 1× antibiotic-antimycotic (Invitrogen). DNA transfection into both cells was performed using the FuGENE HD transfection reagent (Roche) according to the manufacturer's instructions.

Fly lines used for obtaining embryos with different *hb* gene copies were: *Df(3R)p13, red[1], e[1]/TM3, Sb[1]* (for *1×hb* embryos; Bloomington *Drosophila* Stock 1943); *w[1118]* (for *2× hb* embryos); *KG-W25* (for *4×hb* embryos; a line kindly provided by Dr. James W. Posakony [45]). For the identification of *1×hb* embryos, we introduced a marked balancer chromosome (*TM3, hb-lacZ*, which was derived from line #76 of the Bloomington *Drosophila* Stock Center) into the deficiency line to establish the *Df(3R)p13, red[1], e[1]/TM3, hb-lacZ, Sb[1], Ser[1]* flies. When these males were crossed to *w[1118]* virgin females, the desired *1×hb* embryos were identified by a lack of *lacZ* products. Females that contain different *bcd* gene copy numbers were: *Sp/CyO; bcd[E1]/TM6B* (for *1×bcd* embryos); *w[1118]* (for *2×bcd*

embryos); *Sp/CyO-bcd+*; *Dr/TM6B* (for *3×bcd* embryos; derived from a line kindly provided by Dr. Gary Struhl [4]). The fly line *dmpd^EY08992* (Bloomington *Drosophila* Stock 17518) was used in P-element mediated imprecise excision to obtain the deletion allele *dmpd^6-3*. The fly line *w^1118; Df(2R)BSC303/Cyo* (Bloomington *Drosophila* Stock 23686) is a deficiency line covering the entire *dmpd* coding region.

Immunocytochemistry and reporter assay

Immunocytochemistry was performed [10] by first transfecting the HA-Dmpd expressing plasmid into *Drosophila* S2 cells on a Lab-Tek II chamber slide. After fixing by 4% formaldehyde for 15 min at RT, cells were permeabilized by 0.3% Triton X-100 and incubated with anti-HA antibody (1:100 dilution) at 4°C overnight. After washing, Alexa Fluor®488 goat anti-mouse IgG (1:400 dilution) was added to cells and incubated for 2 hrs at RT. TO-PRO-3 dye (1 μM) was added to stain DNA for 15 min at RT and, after washing, images were taken under confocal microscopy.

Reporter assays were performed [70] by first transfecting *Drosophila* S2 cells with the *hb-CAT* reporter plasmid, the HA-Bcd expressing plasmid, the *copia-lacZ* internal control plasmid, along with the FLAG-Dmpd expressing plasmid (or pAc5.1/V5-His C as control). After 40 hrs post transfection, cells were harvested and lysed in 0.5% Triton X-100 by three freeze-thaw cycles. The lysates were added to a 150 μl mixture containing 0.2M Tris-HCl, pH 7.5, 1.6mM acetyl CoA (Sigma) and 0.25 μCi ^{14}C-Chloramphenicol (PerkinElmer), and incubated for 1hr at 37 °C. The amount of the lysate mixture used was adjusted by the transfection efficiency, which was evaluated by the β-galactosidase activity in the lysate. The products were extracted by adding 1ml ethyl acetate, dried by a Speed Vac Concentrator and resuspended in 20 μl ethyl acetate. 10μl products were spotted in a plate for thin-layer chromatography (TLC) and allowed to migrate up the TLC plate with the chloroform: methanol (95:5) solvent. After it is air-dried, the TLC plate was exposed to a storage phosphor screen (Molecular Dynamics) overnight. The screen was then scanned by the Storm 860 imaging scanner (Amersham) and intensities were quantified using the ImageQuant software.

Co-immunoprecipitation and Western blots

Co-immunoprecipitation was performed [10] in HEK 293T cells that had been co-transfected with plasmids expressing HA-Bcd and FLAG-Dmpd. The transfected cells were collected and lysed in the whole cell extract buffer (400 mM KCl, 10 mM Na_2HPO_4, 1 mM EDTA, 1 mM dithiothreitol, 10% glycerol, 1 mM phenylmethylsulfonyl fluoride, 0.5% NP-40 with complete protease inhibitor cocktail). Appropriate antibodies and protein G Sepharose™ 4 fast flow beads were added to the extracts and mixtures were incubated overnight at 4 °C. After washing with the whole cell extract buffer, the beads were boiled in 1 × SDS-PAGE loading buffer (50 mM Tris-HCl, pH 6.8, 100 mM dithiothreitol, 2% SDS, 10% glycerol, 0.1% bromophenol blue). Samples were loaded and separated by SDS-PAGE and transferred to Immun-Blot™ PVDF membrane (Bio-Rad). The membrane was then incubated with appropriate primary antibodies (1:1000 dilution) followed by HRP-conjugated secondary antibodies (GE Healthcare, 1:2000 dilution). Protein signals were visualized by the ECL plus Western blotting detection reagents (GE Healthcare). HA-tagged

and FLAG-tagged proteins were immunoprecipitated and detected by anti-HA (Covance) and anti-FLAG (Sigma) antibodies, respectively. Uncropped gel scans for Western blot results are shown in Supplementary Fig. S13.

Imaging of stained embryos and data analysis

All embryos used in this study were collected at 25°C. Procedures of fluorescence *in situ* hybridization (FISH) to detect mRNA (*hb*, *lacZ* and *eve*), immunostaining to detect Bcd protein and intron staining to detect *hb* nascent transcripts in the fixed embryos were as follows [10,11,44]. Fixed embryos were hydrated in stepwise to PBST buffer and post-fixed by 10% formaldehyde for 20 min. After washing with PBST, embryos were transferred to the Hb-B buffer (50% formamide, 5× SSC, 0.3% SDS, and 0.1% Tween 20) in stepwise and incubated with Hb-A buffer (50% formamide, 5× SSC, 0.3% SDS, 0.1% Tween 20, 50 μg/ml heparin, 10 μg/ml yeast tRNA, and 100 μg/ml denatured salmon sperm DNA) containing the appropriated Digoxigenin-11-UTP labeled RNA probes at 60 °C overnight. For anti-Bcd immunostaining, the overnight incubation at 60 °C was carried out in Hb-B buffer. The embryos were transferred back in stepwise to PBST buffer at 60 °C and washed with PBST at RT for 5 times, followed by incubations first with 1.75× blocking buffer (Roche) for a half hour and then with the primary antibodies (1:300 dilution of anti-Digoxigenin monoclonal antibody (Roche) for FISH and intron staining or 1:100 dilution of anti-Bcd antibodies (Santa Cruz) for immune-staining) at 4 °C overnight. After washing with PBST buffer, the embryos were incubated with 1.75× blocking buffer for a half hour and then secondary fluorescence-conjugated secondary antibodies (1:400 dilution) for 1hr at RT. Individual embryos were assigned to a time class according to their mean nuclear height measured from the "lateral" side of the midsagittal images [44]. Images for FISH and anti-Bcd immune-staining were captured with the Zeiss Imager Z1 ApoTome microscope on the midsagittal plane [10,11], and those for intron staining were captured under confocal microscopy on the surface of the nuclear monolayer with serial *z*-sections [44]. For FISH data analyses [10,44], we first extracted raw intensities from the cytoplasmic layer using a circular window of 61 pixels to scan along the dorsal edge immediately outside of the nuclear layer (basally for *hb*; apically for *eve*). The scanning intervals were 2% EL for *hb* or 1% EL for *eve* along the AP axis of the embryo. The background used for subtraction in an individual embryo was the average intensity at a non-expression region (between the anterior domain and posterior stripe for *hb*; the anterior 10% EL domain for *eve*). To extract raw Bcd intensities from immuno-stained embryos, a circular window was used to scan the dorsal nuclear layer of the midsagittal images. To generate an intensity profile as a function of absolute distance from the anterior (x) or relative AP position (x/L), the scanning intervals were set as either ~12 μm or 2% EL. To calculate ρ from intron staining data, all nuclei in an individual embryo were grouped into bins of the size of 2% EL along the AP axis. The average intron dot number per nucleus within each bin was calculated and defined as ρ. The measurement of embryo length required stitching two sets of images that were captured separately for the anterior and posterior parts of an embryo. The anterior ~60% EL domain for each embryo (where the intron staining data were used in ρ calculations) was captured by a single set of images. To calculate the length constant (λ) of the Bcd gradient profile from an individual embryo, the equation of $B = A \times e^{-x/\lambda} + C$ was used to fit the experimentally extracted data [10]. To avoid data from the non-exponential anterior region and the error-prone

posterior region, fitting was performed within the *x/L* range of 0.2-0.9. Data fitting and other statistical analyses including Student's *t*-tests (two-tailed) were performed using the Matlab software (MathWorks).

Supplementary Material

Refer to Web version on PubMed Central for supplementary material.

Acknowledgements

References

1. Driever W, Nusslein-Volhard C. A gradient of bicoid protein in Drosophila embryos. Cell. 1988; 54:83–93. [PubMed: 3383244]

2. Ephrussi A, St Johnston D. Seeing is believing: the bicoid morphogen gradient matures. Cell. 2004; 116:143–152. [PubMed: 14744427]

3. Driever W, Nusslein-Volhard C. The bicoid protein is a positive regulator of hunchback transcription in the early Drosophila embryo. Nature. 1989; 337:138–143. [PubMed: 2911348]

4. Struhl G, Struhl K, Macdonald PM. The gradient morphogen bicoid is a concentration-dependent transcriptional activator. Cell. 1989; 57:1259–1273. [PubMed: 2567637]

5. Bender M, Horikami S, Cribbs D, Kaufman TC. Identification and expression of the gap segmentation gene hunchback in Drosophila melanogaster. Dev Genet. 1988; 9:715–732. [PubMed: 2849517]

6. Tautz D, et al. Finger Protein of Novel Structure Encoded by Hunchback, a 2nd Member of the Gap Class of Drosophila Segmentation Genes. Nature. 1987; 327:383–389.

7. Driever W, Nusslein-Volhard C. The bicoid protein determines position in the Drosophila embryo in a concentration-dependent manner. Cell. 1988; 54:95–104. [PubMed: 3383245]

8. Berleth T, et al. The role of localization of bicoid RNA in organizing the anterior pattern of the Drosophila embryo. EMBO J. 1988; 7:1749–1756. [PubMed: 2901954]

9. Liu J, He F, Ma J. Morphogen gradient formation and action: insights from studying Bicoid protein degradation. Fly (Austin). 2011; 5:242–246. [PubMed: 21525787]

10. Liu J, Ma J. Fates-shifted is an F-box protein that targets Bicoid for degradation and regulates developmental fate determination in Drosophila embryos. Nat Cell Biol. 2011; 13:22–29. [PubMed: 21170036]

11. He F, et al. Probing intrinsic properties of a robust morphogen gradient in Drosophila. Dev Cell. 2008; 15:558–567. [PubMed: 18854140]

12. Schaeffer V, Janody F, Loss C, Desplan C, Wimmer EA. Bicoid functions without its TATA-binding protein-associated factor interaction domains. Proc Natl Acad Sci U S A. 1999; 96:4461–4466. [PubMed: 10200284]

13. Zhao C, et al. The activity of the Drosophila morphogenetic protein Bicoid is inhibited by a domain located outside its homeodomain. Development. 2002; 129:1669–1680. [PubMed: 11923203]

14. Liu J, Ma J. Drosophila Bicoid is a substrate of sumoylation and its activator function is subject to inhibition by this post-translational modification. FEBS Lett. 2012; 586:1719–1723. [PubMed: 22584054]

15. Driever W, Ma J, Nusslein-Volhard C, Ptashne M. Rescue of bicoid mutant Drosophila embryos by bicoid fusion proteins containing heterologous activating sequences. Nature. 1989; 342:149–154. [PubMed: 2509940]

16. Simpson-Brose M, Treisman J, Desplan C. Synergy between the hunchback and bicoid morphogens is required for anterior patterning in Drosophila. Cell. 1994; 78:855–865. [PubMed: 8087852]

17. Arnosti DN, Barolo S, Levine M, Small S. The eve stripe 2 enhancer employs multiple modes of transcriptional synergy. Development. 1996; 122:205–214. [PubMed: 8565831]

18. Ho MS, Tsai PI, Chien CT. F-box proteins: the key to protein degradation. J Biomed Sci. 2006; 13:181–191. [PubMed: 16463014]

19. Cardozo T, Pagano M. The SCF ubiquitin ligase: insights into a molecular machine. Nat Rev Mol Cell Biol. 2004; 5:739–751. [PubMed: 15340381]

20. Skaar JR, Pagan JK, Pagano M. SnapShot: F box proteins I. Cell. 2009; 137:1160–1161. 1160. [PubMed: 19524517]

21. Skaar JR, D'Angiolella V, Pagan JK, Pagano M. SnapShot: F Box Proteins II. Cell. 2009; 137:1358–1351. 1358. [PubMed: 19563764]

22. Deshaies RJ. SCF and Cullin/Ring H2-based ubiquitin ligases. Annu Rev Cell Dev Biol. 1999; 15:435–467. [PubMed: 10611969]

23. Freed E, et al. Components of an SCF ubiquitin ligase localize to the centrosome and regulate the centrosome duplication cycle. Genes Dev. 1999; 13:2242–2257. [PubMed: 10485847]

24. Seol JH, et al. Cdc53/cullin and the essential Hrt1 RING-H2 subunit of SCF define a ubiquitin ligase module that activates the E2 enzyme Cdc34. Genes Dev. 1999; 13:1614–1626. [PubMed: 10385629]

25. Muratani M, Kung C, Shokat KM, Tansey WP. The F box protein Dsg1/Mdm30 is a transcriptional coactivator that stimulates Gal4 turnover and cotranscriptional mRNA processing. Cell. 2005; 120:887–899. [PubMed: 15797387]

26. Conaway RC, Brower CS, Conaway JW. Emerging roles of ubiquitin in transcription regulation. Science. 2002; 296:1254–1258. [PubMed: 12016299]

27. Lipford JR, Deshaies RJ. Diverse roles for ubiquitin-dependent proteolysis in transcriptional activation. Nat Cell Biol. 2003; 5:845–850. [PubMed: 14523392]

28. von der Lehr N, et al. The F-box protein Skp2 participates in c-Myc proteosomal degradation and acts as a cofactor for c-Myc-regulated transcription. Mol Cell. 2003; 11:1189–1200. [PubMed: 12769844]

29. Kim SY, Herbst A, Tworkowski KA, Salghetti SE, Tansey WP. Skp2 regulates Myc protein stability and activity. Mol Cell. 2003; 11:1177–1188. [PubMed: 12769843]

30. Kimbrel EA, Kung AL. The F-box protein beta-TrCp1/Fbw1a interacts with p300 to enhance beta-catenin transcriptional activity. J Biol Chem. 2009; 284:13033–13044. [PubMed: 19297328]

31. Hsu T, McRackan D, Vincent TS, Gert de Couet H. Drosophila Pin1 prolyl isomerase Dodo is a MAP kinase signal responder during oogenesis. Nat Cell Biol. 2001; 3:538–543. [PubMed: 11389437]

32. Ma X, Yuan D, Diepold K, Scarborough T, Ma J. The Drosophila morphogenetic protein Bicoid binds DNA cooperatively. Development. 1996; 122:1195–1206. [PubMed: 8620846]

33. Yuan D, Ma X, Ma J. Recognition of multiple patterns of DNA sites by Drosophila homeodomain protein Bicoid. J Biochem. 1999; 125:809–817. [PubMed: 10101296]

34. Sadowski I, Ma J, Triezenberg S, Ptashne M. GAL4-VP16 is an unusually potent transcriptional activator. Nature. 1988; 335:563–564. [PubMed: 3047590]

35. Crauk O, Dostatni N. Bicoid determines sharp and precise target gene expression in the Drosophila embryo. Curr Biol. 2005; 15:1888–1898. [PubMed: 16271865]

36. Perry MW, Bothma JP, Luu RD, Levine M. Precision of hunchback expression in the Drosophila embryo. Curr Biol. 2012; 22:2247–2252. [PubMed: 23122844]

37. Bergmann S, et al. 2007; 5:e46.

38. Houchmandzadeh B, Wieschaus E, Leibler S. Establishment of developmental precision and proportions in the early Drosophila embryo. Nature. 2002; 415:798–802. [PubMed: 11845210]

39. Jaeger J, et al. Dynamic control of positional information in the early Drosophila embryo. Nature. 2004; 430:368–371. [PubMed: 15254541]

40. Gregor T, Tank DW, Wieschaus EF, Bialek W. Probing the limits to positional information. Cell. 2007; 130:153–164. [PubMed: 17632062]

41. Jaeger J. The gap gene network. Cell Mol Life Sci. 2011; 68:243–274. [PubMed: 20927566]

42. Chen H, Xu Z, Mei C, Yu D, Small S. A system of repressor gradients spatially organizes the boundaries of bicoid-dependent target genes. Cell. 2012; 149:618–629. [PubMed: 22541432]

43. He F, Ren J, Wang W, Ma J. Evaluating the Drosophila Bicoid morphogen gradient system through dissecting the noise in transcriptional bursts. Bioinformatics. 2012; 28:970–975. [PubMed: 22302571]

44. Liu J, Ma J. Uncovering a dynamic feature of the transcriptional regulatory network for anterior-posterior patterning in the Drosophila embryo. PLoS One. 2013; 8:e62641. [PubMed: 23646132]

45. Margolis JS, et al. Posterior stripe expression of hunchback is driven from two promoters by a common enhancer element. Development. 1995; 121:3067–3077. [PubMed: 7555732]

46. Struhl G, Johnston P, Lawrence PA. Control of Drosophila body pattern by the hunchback morphogen gradient. Cell. 1992; 69:237–249. [PubMed: 1568245]

47. Payankaulam S, Arnosti DN. Gene regulation: boundaries within limits. Curr Biol. 2008; 18:R653–R655. [PubMed: 18682204]

48. Yu D, Small S. Precise registration of gene expression boundaries by a repressive morphogen in Drosophila. Curr Biol. 2008; 18:868–876. [PubMed: 18571415]

49. Bothma JP, Magliocco J, Levine M. The snail repressor inhibits release, not elongation, of paused Pol II in the Drosophila embryo. Curr Biol. 2011; 21:1571–1577. [PubMed: 21920753]

50. Ma J. Crossing the line between activation and repression. Trends Genet. 2005; 21:54–59. [PubMed: 15680515]

51. Geng F, Wenzel S, Tansey WP. Ubiquitin and proteasomes in transcription. Annu Rev Biochem. 2012; 81:177–201. [PubMed: 22404630]

52. Kodadek T, Sikder D, Nalley K. Keeping transcriptional activators under control. Cell. 2006; 127:261–264. [PubMed: 17055428]

53. Muratani M, Tansey WP. How the ubiquitin-proteasome system controls transcription. Nat Rev Mol Cell Biol. 2003; 4:192–201. [PubMed: 12612638]

54. Wartlick O, Kicheva A, Gonzalez-Gaitan M. Morphogen gradient formation. Cold Spring Harb Perspect Biol. 2009; 1:a001255. [PubMed: 20066104]

55. Dui W, Lu W, Ma J, Jiao R. A systematic phenotypic screen of F-box genes through a tissue-specific RNAi-based approach in Drosophila. J Genet Genomics. 2012; 39:397–413. [PubMed: 22884096]

56. Deng J, Wang W, Lu LJ, Ma J. A two-dimensional simulation model of the bicoid gradient in Drosophila. PLoS One. 2010; 5:e10275. [PubMed: 20422054]

57. Cheung D, Miles C, Kreitman M, Ma J. Scaling of the Bicoid morphogen gradient by a volume-dependent production rate. Development. 2011; 138:2741–2749. [PubMed: 21613328]

58. Cheung D, Miles C, Kreitman M, Ma J. Adaptation of the length scale and amplitude of the Bicoid gradient profile to achieve robust patterning in abnormally large Drosophila melanogaster embryos. Development. 2013 in press.

59. Porcher A, et al. The time to measure positional information: maternal hunchback is required for the synchrony of the Bicoid transcriptional response at the onset of zygotic transcription. Development. 2010; 137:2795–2804. [PubMed: 20663819]

60. Foe VE, Alberts BM. Studies of nuclear and cytoplasmic behaviour during the five mitotic cycles that precede gastrulation in Drosophila embryogenesis. J Cell Sci. 1983; 61:31–70. [PubMed: 6411748]

61. He F, Ma J. A spatial point pattern analysis in Drosophila blastoderm embryos evaluating the potential inheritance of transcriptional states. PLoS One. 2013; 8:e60876. [PubMed: 23593336]

62. Shermoen AW, O'Farrell PH. Progression of the cell cycle through mitosis leads to abortion of nascent transcripts. Cell. 1991; 67:303–310. [PubMed: 1680567]

63. Lagha M, et al. Paused Pol II Coordinates Tissue Morphogenesis in the Drosophila Embryo. Cell. 2013; 153:976–987. [PubMed: 23706736]

64. Lucas T, et al. Live Imaging of Bicoid-Dependent Transcription in Drosophila Embryos. Curr Biol. 2013; 23:2135–2139. [PubMed: 24139736]

65. Garcia HG, Tikhonov M, Lin A, Gregor T. Quantitative Imaging of Transcription in Living Drosophila Embryos Links Polymerase Activity to Patterning. Curr Biol. 2013; 23:2140–2145. [PubMed: 24139738]

66. Bertrand E, et al. Localization of ASH1 mRNA particles in living yeast. Mol Cell. 1998; 2:437–445. [PubMed: 9809065]

67. Forrest KM, Gavis ER. Live imaging of endogenous RNA reveals a diffusion and entrapment mechanism for nanos mRNA localization in Drosophila. Curr Biol. 2003; 13:1159–1168. [PubMed: 12867026]

68. Little SC, Tikhonov M, Gregor T. Precise developmental gene expression arises from globally stochastic transcriptional activity. Cell. 2013; 154:789–800. [PubMed: 23953111]

69. He F, Ren J, Wang W, Ma J. A multiscale investigation of bicoid-dependent transcriptional events in Drosophila embryos. PLoS One. 2011; 6:e19122. doi:10.1371/journal.pone.0019122. [PubMed: 21544208]

70. Zhao C, Dave V, Yang F, Scarborough T, Ma J. Target selectivity of Bicoid is dependent on non-consensus site recognition and protein-protein interaction. Mol. Cell. Biol. 2000; 20:8112–8123. [PubMed: 11027281]
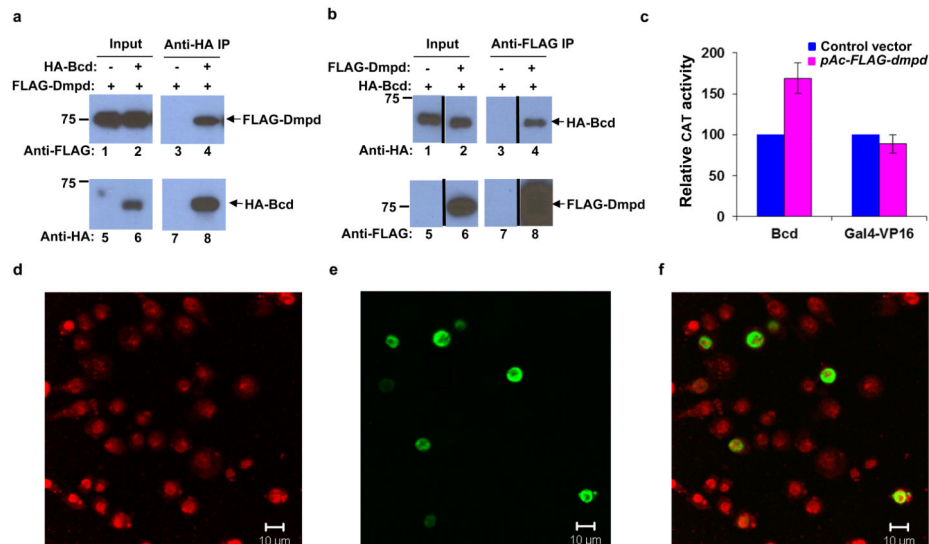
Figure 1. Dmpd is a nuclear factor that stimulates Bcd-dependent reporter activity in cells
(**a** and **b**) FLAG-Dmpd interacts with HA-Bcd. Coimmunopreciptiation (co-IP) experiments were performed to detect the interaction between FLAG-Dmpd and HA-Bcd. Here, extracts from HEK293T cells expressing the indicated fusion proteins were subject to co-IP by the indicated antibodies, followed by Western blot detections by the indicated antibodies. Lanes 5 and 6 in these panels document the specificity of the antibodies used in our study.
(**c**) Bcd activity is stimulated by Dmpd. Reporter assays were performed in *Drosophila* S2 cells to evaluate the impact of Dmpd expression on CAT reporter activity. For each set of experiments, CAT activities were normalized to those obtained from cells without Dmpd expression (set as 100). Data shown are from three independent sets of experiments, with standard deviation (sd) shown for Dmpd-expressing cells.
(**d-f**) Nuclear localization of Dmpd. A plasmid expressing the HA-tagged Dmpd protein (HA-Dmpd) was transfected into S2 cells. Immunocytochemistry experiments were then performed to evaluate its sub-cellular localization through the use of the anti-HA antibody (**e**). To-pro-3 was used to counterstain the nucleus (**d**). Panel **f** is a merge of images shown in panels **d** and **e**. Scale bar is 10 μm.
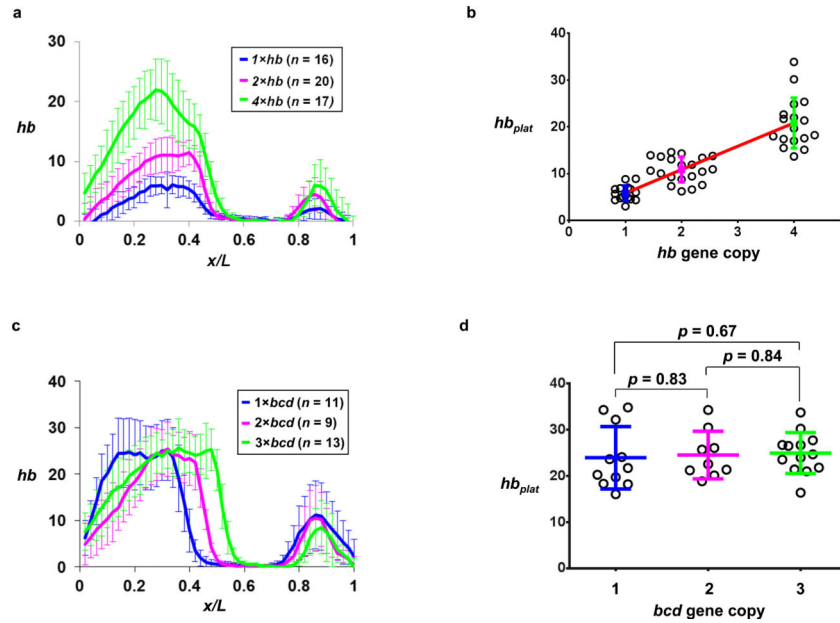
Figure 2. Establishing a platform for quantifying the amplitude of *hb* transcription

(**a**) Shown are the mean profiles (with sd shown) of un-normalized *hb* mRNA FISH intensities (in arbitrary units) from embryos that have one, two, or four copies of the *hb* gene. The mean and sd of x_{hb} expressed as fractional embryo length are: 0.435 ± 0.013, 0.445 ± 0.013 and 0.454 ± 0.019 for $1\times$, $2\times$ and $4\times hb$ embryos, respectively ($n = 16, 20$ and 17). These results show that x_{hb} remains largely insensitive to changes in *hb* copy number in our experimental system; a relatively minor shift might be related to the limitations inherent to experimental detections [35].

(**b**) Shown are hb_{plat} values (in arbitrary units) in individual embryos with different copies of the *hb* gene. The mean and sd are also shown in the figure ($n = 16, 20$ and 17 for $1\times$, $2\times$ and $4\times hb$ embryos, respectively). The linear fit between hb_{plat} and *hb* gene copy number is shown as a red line in the figure.

(**c**) Shown are the mean profiles of un-normalized *hb* mRNA FISH intensities in embryos from mothers with one, two, or three copies of *bcd*. The mean and sd of x_{hb} expressed as fractional embryo length are: 0.373 ± 0.013, 0.446 ± 0.009, and 0.510 ± 0.010 for $1\times$, $2\times$ and $3\times bcd$ embryos, respectively ($n = 11, 9$, and 13).

(**d**) Shown are hb_{plat} values in individual embryos from mothers with different copies of *bcd*. The mean and sd of hb_{plat} are: 23.93 ± 6.75, 24.51 ± 5.13, and 24.94 ± 4.42 for $1\times$, $2\times$ and $3\times bcd$ embryos, respectively ($n = 11, 9$, and 13). *p* values (obtained from Student's *t*-tests and shown in the figure) reveal no significant differences.
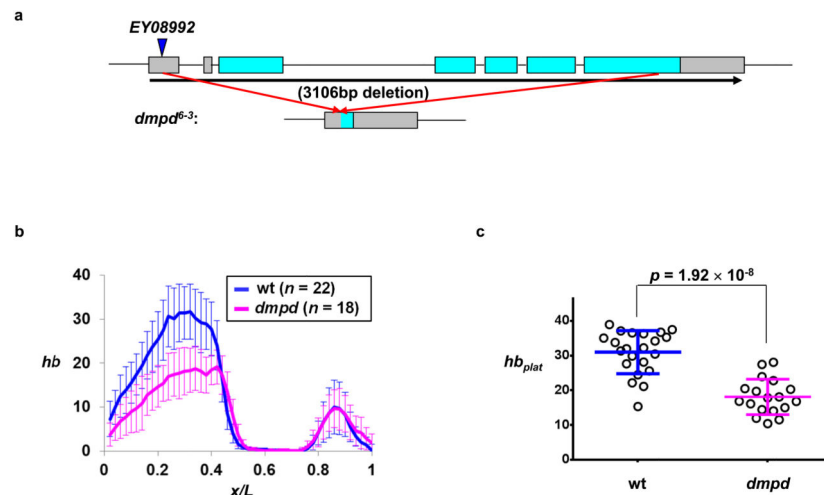
Figure 3. *hb* mRNA level is reduced in *dmpd* embryos

(**a**) A schematic diagram showing the deletion caused by the *dmpd*[6-3] allele. The boxes represent exons with the annotated open reading frame in cyan and the un-translated regions in grey. The blue arrow shows the P-element insertion site for *dmpd*[EY08992].

(**b**) Shown are the mean profiles of un-normalized *hb* mRNA FISH intensities in wt and *dmpd* embryos ($n = 22$ and 18, respectively). Note that the level of the Bcd-independent posterior *hb* expression domain remains unaffected in *dmpd* embryos ($p = 0.93$, Student's *t*-test); see text and panel **c** legend for further details). The mean and sd of x_{hb} expressed as fractional embryo length are: 0.433 ± 0.012 and 0.462 ± 0.018 for wt and *dmpd* embryos, respectively ($p = 4.8 \times 10^{-7}$, Student's *t*-test).

(**c**) Shown are hb_{plat} values in individual wt and *dmpd* embryos ($n = 22$ and 18, respectively). Unlike the significant amplitude reduction for the Bcd-activated anterior *hb* expression domain shown in this figure, the amplitude of the Bcd-independent posterior *hb* expression domain, hb_{post} (defined as the average FISH intensities at the three peak positions of the posterior domain), is insensitive to *dmpd* mutation.
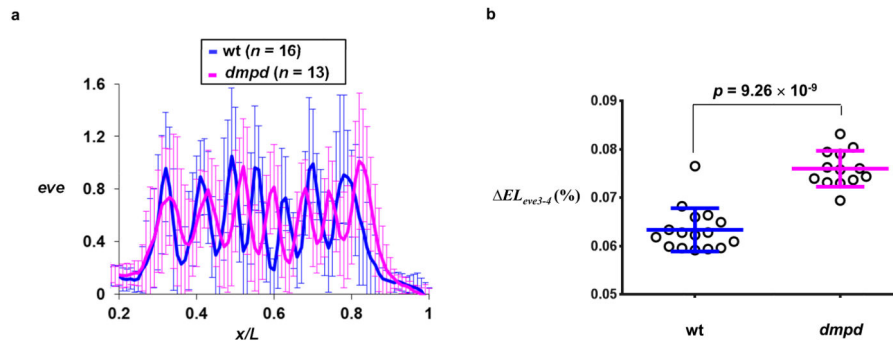
Figure 4. The spacing between *eve* stripes 3 and 4 is sensitive to the *dmpd* mutation
(**a**) Shown are the normalized mean intensity profiles of *eve* in wt and *dmpd* embryos (n = 16 and 13, respectively).

(**b**) Shown is the calculated distance between *eve* stripes 3 and 4 in each individual wt and *dmpd* embryos (n = 16 and 13, respectively). The distance values shown are expressed as percentage of embryo length. Also shown are mean and sd for these two groups, along with the p value obtained from Student's *t*-test.
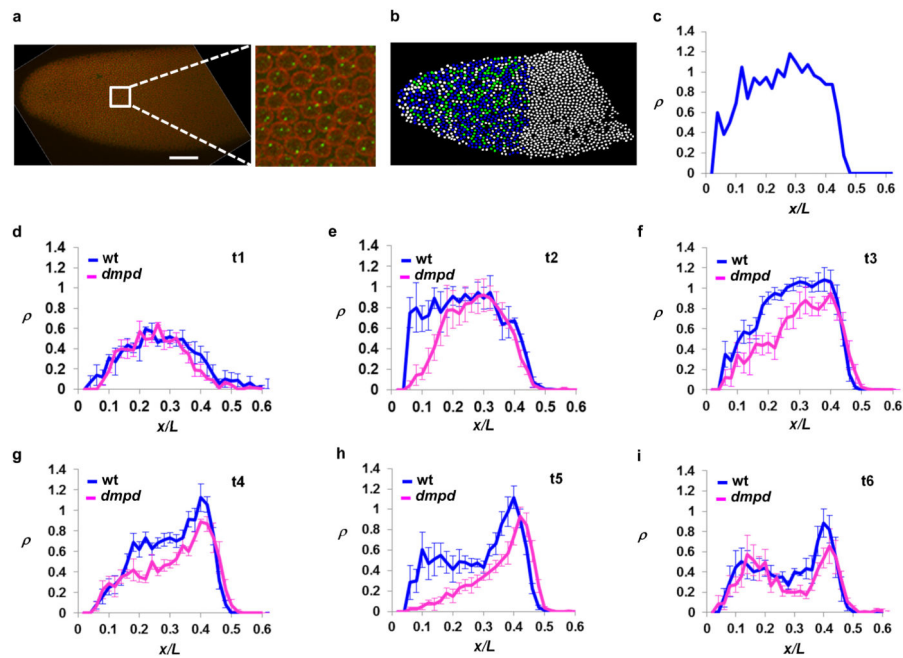
Figure 5. The transcribing probability near Bcd-responsive promoter of *hb* is decreased in *dmpd* embryos

(**a**) Shown is an image of *hb* intron staining from a cycle 14 embryo. Nuclear envelope is shown in red and intron dots in green. Scale bar, 50μm. A magnified view of a section of the expression domain is shown on the right side of this panel.

(**b**) Shown is a computer-processed image of panel **a**. Here each of the identified nuclei is shown in a color according to the number of intron dots detected inside. White, blue and green represent zero, one and two intron dots detected, respectively.

(**c**) Shown is the plot of ρ as a function of *x/L* based on panel **b**.

(**d-i**) Shown are the mean ρ profiles from wt and *dmpd* embryos at time classes t1-t6. The mean and sd of ρ_{plat} for t1-t6 time classes are: 0.50 ± 0.07; 0.84 ± 0.04; 1.03 ± 0.08; 0.71 ± 0.14; 0.52 ± 0.10; 0.34 ± 0.03 for wt embryos ($n = 3, 3, 7, 7, 5$ and 4, respectively) and 0.51 ± 0.11; 0.86 ± 0.25; 0.79 ± 0.21; 0.54 ± 0.06; 0.38 ± 0.12; 0.23 ± 0.05 for *dmpd* embryos ($n = 3, 4, 5, 5, 5$ and 4), respectively. The *p* values (from Student's *t*-tests) between wt and *dmpd* embryos for t1-t6 time classes are: 0.93; 0.92; 0.016; 0.028; 0.078; 0.0087, respectively. The mean ρ at *x/L* ~0.15 (which is located outside of the plateau domain for calculating ρ_{plat}) appears higher in *dmpd* embryos than in wt embryos at t6 (panel **i**); this is likely caused by an "outlier" *dmpd* embryo that has a very high level of ρ at this location (see Fig. S8f).
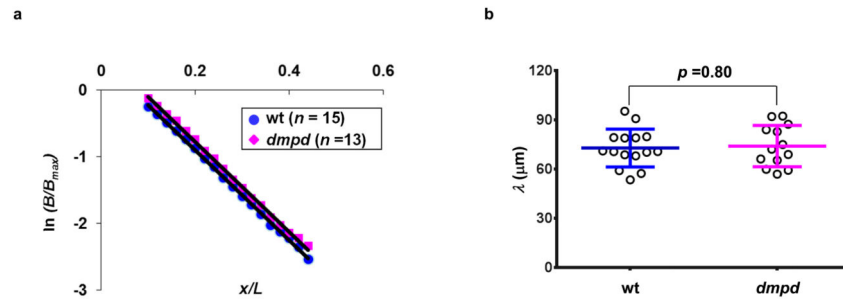
Figure 6. Similar length constant of the Bcd gradient profiles in wt and *dmpd* embryos
(**a**) Shown are mean Bcd gradient profiles from wt and *dmpd* embryos plotted as $ln(B/B_{max})$ against AP position x/L. Here both B and B_{max} are background-adjusted intensities without any further adjustments. The solid lines representing linear fits ($y = -6.78x + 0.46$, R squared for linear regression; $R^2 = 0.999$ for wt embryos; $y = -6.77x + 0.58$; R squared for linear regression, $R^2 = 0.998$ for *dmpd* embryos).

(**b**) Shown are calculated λ values of Bcd gradient profiles from individual wt and *dmpd* embryos ($n = 15$ and 13, respectively). These values were obtained from fitting the individual Bcd intensity profiles to an exponential function. Shown are mean and sd for these two groups, along with the p value obtained from Student's *t*-test.